

www.afm-journal.de

# Reversing Multidrug-Resistant *Escherichia coli* by Compromising Its BAM Biogenesis and Enzymatic Catalysis through Microwave Hyperthermia Therapy

Congyang Mao, Wanyu Jin, Yiming Xiang, Yizhou Zhu, Jun Wu, Xiangmei Liu,\* Shuilin Wu,\* Yufeng Zheng,\* Kenneth M.C. Cheung, and Kelvin Wai Kwok Yeung\*

Multidrug-resistant (MDR) bacteria are emerging and disseminating rapidly, undoubtedly posing an urgent threat to global public health. One particular concern is that MDR Gram-negative bacteria are immunized to available antibiotics owing to a series of biogenetic effects, including the  $\beta$ -barrel assembly machine (BAM complex) in the outer membrane, MDR efflux pumps, and enzymatic degradation/modification, which are known to induce antibiotic resistance (AbR). Here, this work identifies that the AbR mechanisms of MDR Escherichia coli become compromised and sensitive again to conventional antibiotics, when the temperature of infected tissues is elevated to ≈50 °C in situ. This thought is realized by the microwave-driven poly(lactic-co-glycolic acid) microparticles that may effectively convert electromagnetic radiation to thermal energy. The microwave hyperthermia (MWH) therapy not only interrupts the essential surface-exposed BamA protein of the BAM complex, but also enhances the permeability of the outer membrane and inhibits the action of MDR efflux pumps. MWH also impairs the hydrogen bond interaction between the catalytic residues of bacterial enzymes and functional groups of antibiotic molecules. Lastly, this work demonstrates these combined inhibitors can revitalize the bactericidal effects of conventional antibiotics in MDR Escherichia coli-associated deep tissue infections.

1. Introduction

Since the serendipitous advent of the first antibiotic, penicillin, in 1929, antibiotics have undeniably been one of the most important discoveries in medical history and have saved hundreds of millions of lives from leading infections that cause severe diseases and death in humankind.[1,2] Over time, the consumption of antibiotics has dramatically increased, directly leading to more antibiotic resistance (AbR), which is the stable and heritable ability of microorganisms to survive and proliferate in the presence of originally sensitive antibiotics at high levels.<sup>[3–5]</sup> The twin trends of increasing AbR and decreasing number of new antibiotics have made drug-resistant pathogen-associated infections a serious global public health menace again.<sup>[6]</sup> Currently, AbR-associated infections kill ≈700 000 people each year worldwide. The number of deaths from AbR is predicted to increase to 10 million by the year 2050, with a global economic burden of 100 trillion USD if no further action is taken to address the threat of AbR.[3,7] Hence, how to overcome AbR has become a challenging scientific question that deserves high priority for investigation.<sup>[8]</sup>

Among all multidrug-resistant (MDR) bacteria, MDR *Escherichia coli* (*E. coli*) has been one of the three concerning pathogens, with critical priority identified by the World Health Organization.<sup>[9,10]</sup> As a Gram-negative bacterium, *E. coli* is protected against toxic environmental factors by its unique outer membrane (OM) structure, which is comprised

C. Mao, W. Jin, Y. Xiang, Y. Zhu, K. M.C. Cheung, K. W. K. Yeung Department of Orthopaedics and Traumatology Li Ka Shing Faculty of Medicine The University of Hong Kong Pokfulam, Hong Kong 999077, China E-mail: wkkyeung@hku.hk

C. Mao, W. Jin, Y. Xiang, Y. Zhu, J. Wu, K. M.C. Cheung, K. W. K. Yeung Shenzhen Key Laboratory for Innovative Technology in Orthopaedic Trauma Department of Orthopaedics and Traumatology The University of Hong Kong-Shenzhen Hospital Shenzhen 518053, China

The ORCID identification number(s) for the author(s) of this article can be found under https://doi.org/10.1002/adfm.202202887.

DOI: 10.1002/adfm.202202887

X. Liu
School of Life Science and Health Engineering
Hebei University of Technology
Xiping Avenue 5340, Beichen District, Tianjin 300401, China
E-mail: liuxiangmei@hebut.edu.cn
S. Wu, Y. Zheng
School of Materials Science and Engineering
Peking University
Beijing 100871, China
E-mail: slwu@pku.edu.cn; yfzheng@pku.edu.cn



FUNCTIONAL

www.afm-journal.de

of an asymmetrical lipid bilayer of phospholipids in the inner leaflet and lipopolysaccharide (LPS) in the outer leaflet and poses a powerful permeability barrier to most antibiotics available in clinics. [11–13] The  $\beta$ -barrel assembly machine (BAM complex), the most important structure in the barrier, facilitates the transportation, insertion, and folding of OM proteins (OMPs), which are essential for the biogenesis of the OM.[14-16] The main component of the BAM complex is the BamA protein that belongs to one of OMPs in which it exposes on bacterial OM surface. Indeed, this protein structure makes the bacteria more vulnerable to toxic environments.[11] Therefore, a powerful and effective antibacterial strategy is to weaken the function of the BAM complex by targeting the correlated BamA protein. The small molecule MRL-494, chimeric peptidomimetic antibiotics, darobactin, and the monoclonal antibody MAB1 are the newly developed antibiotics that can inhibit the assembly of OMPs by targeting the BamA protein. [17–20] However, the development of new antibiotics always lags behind the emergence of new drug-resistant bacteria despite the long time and huge efforts invested.<sup>[7,21,22]</sup>

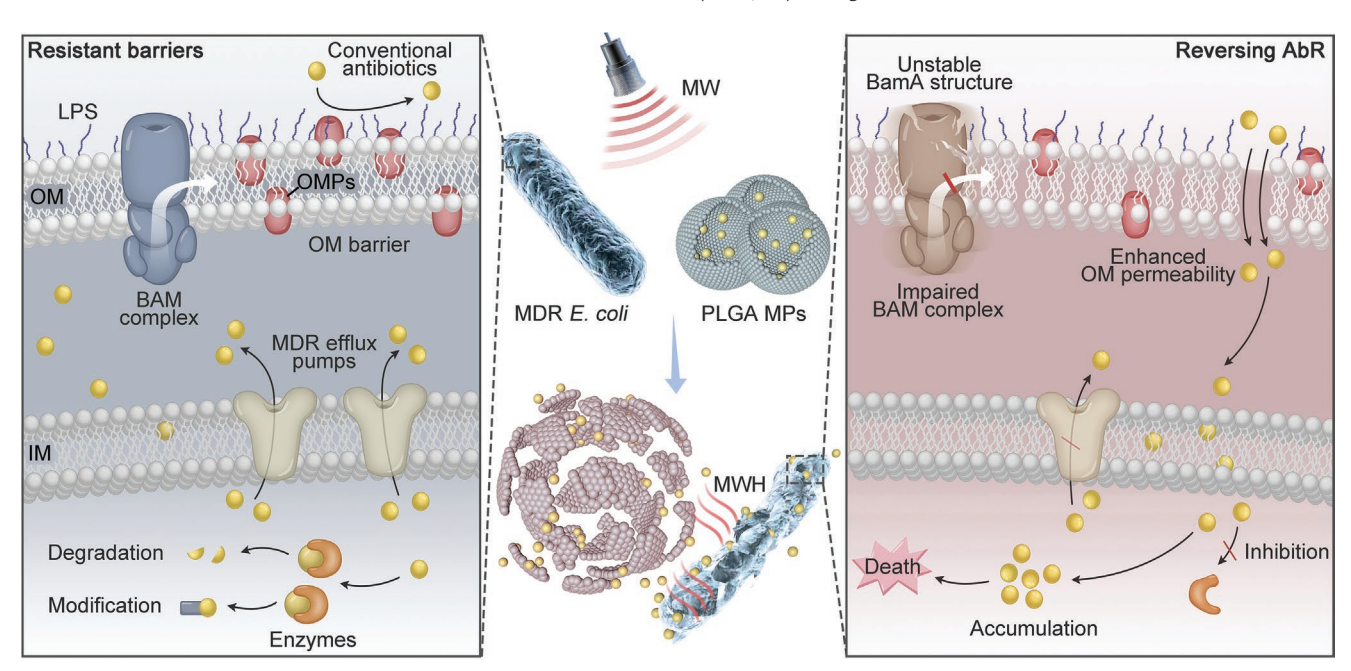
Apart from the inherent antibiotic permeability barrier mediated by the BAM complex, other important mechanisms of MDR *E. coli* that work against antibiotics also include MDR efflux pumps and enzymatic degradation or modification.<sup>[23–25]</sup> A previous study reported that the photothermal effect can weaken the catalytic activity of enzymes in methicillin-resistant *Staphylococcus aureus* (MRSA).<sup>[26]</sup> Hence, we propose to paralyze these barriers through an in situ microwave (MW) hyperthermal (MWH) strategy to effectively facilitate the resensitization of MDR *E. coli* to conventional antibiotics

(Scheme 1). This approach can be realized with custom-made poly(lactic-co-glycolic acid) (PLGA) microparticles (MPs) encapsulated with conventional antibiotics. First, we established a PLGA MPs-induced MWH platform. In fact, the PLGA polymeric segmental motion can effectively convert the mechanical energy of MW motion to kinetic energy (heat) according to the law of energy conservation. We have also combined biochemical, computational, and structural approaches to investigate the role of MWH that appears to potentiate the bactericidal efficacies of the major conventional antibiotics ( $\beta$ -lactam, aminoglycoside, and tetracycline antibiotics) against MDR E. coli by a collaborative strategy, including the structural turbulence of the BAM complex, the functional obstruction of MDR efflux pumps, and the catalytic paralysis of related hydrolytic or modifying enzymes (Scheme 1). Indeed, when MWH combines with the use of commercially available antibiotics, this approach can remarkably diminish the burden of MDR E. coli bacterial infection in deep tissues, such as urinary tract infection (UTI) and peritoneal infection (PI). These findings establish that MWH is a versatile antibiotic potentiator that can be applied to address the current AbR crisis posed by MDR Gram-negative pathogens.

#### 2. Results

#### 2.1. MWH Reverses the AbR of MDR E. coli

We fabricated PLGA MPs with a relatively uniform size ( $\approx$ 20  $\mu$ m) using the water–oil–water double emulsion method



**Scheme 1.** Schematic diagram of the three main resistant barriers in MDR *E. coli* and the mechanisms of overcoming AbR by MWH. MDR *E. coli* is first protected by the OM and inner membrane (IM). The OM contains LPS in the outer leaflet and OMPs spanning the entire OM. The insertion and folding into the OM of OMPs were manipulated by the BAM complex. The main component of the BAM complex is BamA protein. The OM system forms a barrier against traditional antibiotics entering the MDR *E. coli*. In addition, *E. coli* is protected by MDR efflux pumps that extrude drugs from bacterial cells. The enzymatic degradation or modification system help MDR *E. coli* bacteria protect themselves against traditional antibiotics (left). However, we discover that microwave-responsive antibiotics-loaded PLGA MPs release antibiotics and MWH under microwave irradiation (middle). And traditional antibiotics successfully escape from the triple defense systems with the help of MWH by enhancing the BAM complex-mediated OM permeability, downregulating the MDR efflux pump-related proteins, and impairing the synthesis and activities of enzymes (right).

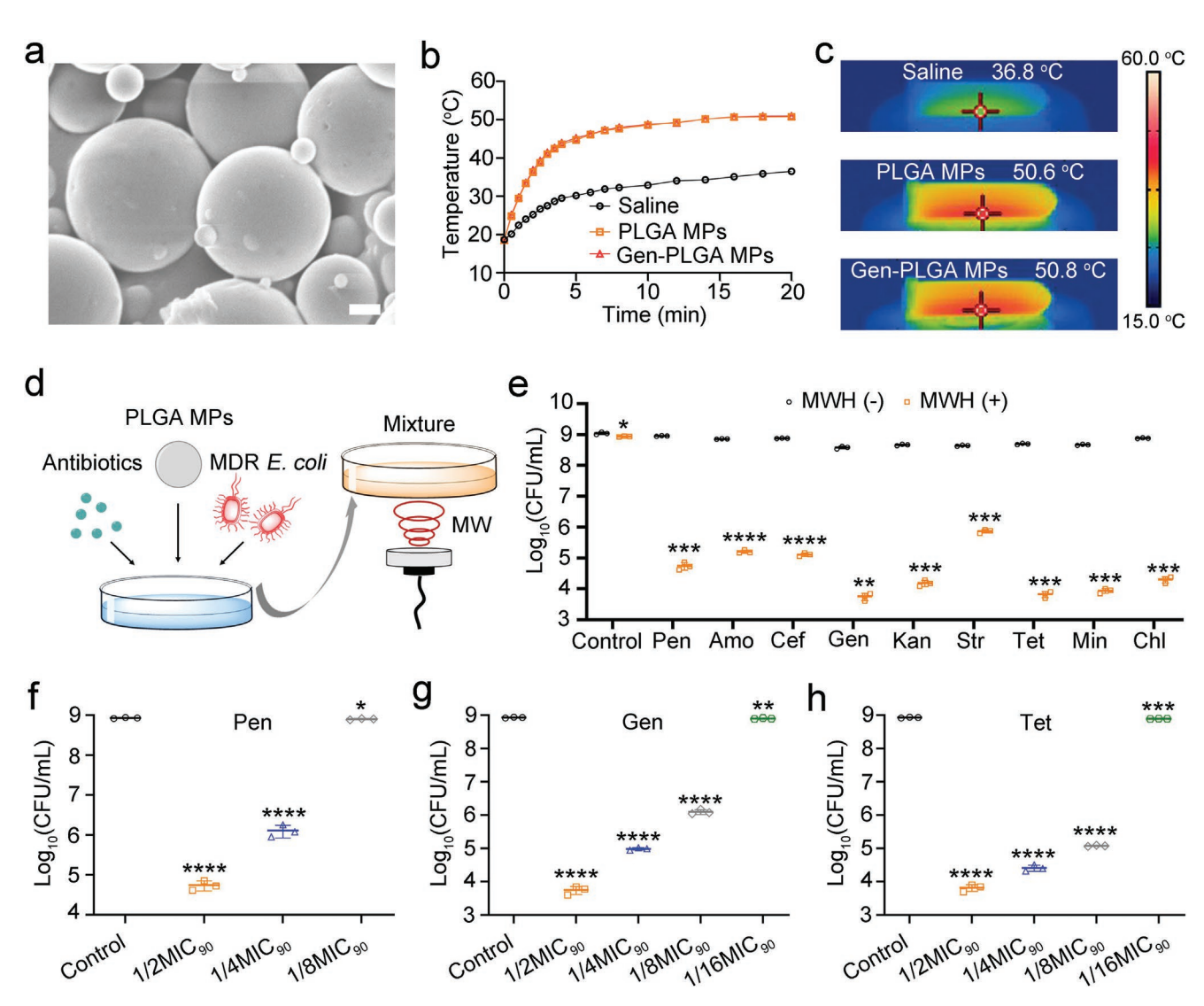


Figure 1. PLGA MPs-induced MWH overcomes antibiotic resistance. a) Scanning electron microscopy image of PLGA MPs. Scale bar: 2 μm. b) Heating curves and c) thermal images of saline, PLGA, and Gen-PLGA MPs saline solutions under MW irradiation for 20 min. d) The antibacterial test model: the mixture of antibiotics, PLGA MPs, and MDR *E. coli* is treated with MW. e) The traditional antibiotics with a concentration of 1/2MIC<sub>90</sub> against MDR *E. coli* without (MWH (–)) or with (MWH (+)) MWH treatment for 10 min. Typical f) β-lactam (Pen), g) aminoglycoside (Gen), and h) tetracycline (Tet) antibiotics with different concentrations against MDR *E. coli*, with MWH treatment for 10 min. Data are taken from independent samples (n = 3), and error bars indicate mean  $\pm$  standard deviations: \*p < 0.05, \*\*p < 0.01, \*\*\*\*p < 0.001, and \*\*\*\*\*p < 0.0001. The statistical analysis was performed using a two-sample Student t-test (e) and a one-way analysis of variance with the Tukey multiple-comparisons test (f–h).

(Figure 1a).<sup>[27]</sup> PLGA MPs were then dispersed in saline and subjected to MW irradiation (4 W, 50% duty cycle). The dispersion of the PLGA MPs showed an excellent heating effect compared with pure saline (Figure 1b). The temperature for the dispersion of PLGA MPs was increased to as high as ≈50 °C within 10 min of MW irradiation and was maintained until the end of the MW irradiation, whereas pure saline was only heated up to ≈37 °C during the entire MW irradiation process. Interestingly, the heating curve of gentamycin-loaded PLGA MPs (Gen-PLGA MPs) almost followed the trend of the pure PLGA MPs, indicating that the loaded drug would not intervene the heating effect induced by MWH. After 20 min of MW irradiation, the real-time temperature of saline was recorded as 36.8 °C, whereas the dispersion of PLGA and Gen-PLGA MPs

reached to 50.6 and 50.8 °C, respectively (Figure 1c), which was biosafe for healthy tissues and far below the minimum temperature (60 °C) to cause damage. $^{[28]}$ 

We further discovered that MWH effectively overcame AbR. First, the Clinical and Laboratory Standards Institute (CLSI) broth microdilution method was used to determine the minimal inhibitory concentration (MIC) of conventional antibiotics within the range of 0.016–8.00 mg mL<sup>-1</sup>, in which at least 90% of the pathogens were inhibited (MIC<sub>90</sub>; Table S1, Supporting Information). After adding PLGA MPs and 1/2MIC<sub>90</sub> concentration of antibiotics into the MDR *E. coli* bacterial culture medium and irradiating the mixture under MW (4 W, 50% duty cycle) for 10 min (Figure 1d), we observed a 4- to 6-log<sub>10</sub> reduction in colony-forming units (CFUs) against MDR *E. coli* by the



www.afm-iournal.de

ADVANCED FUNCTIONAL MATERIALS

major traditional antibiotics, including penicillin (Pen), amoxicillin (Amo), ceftriaxone (Cef), gentamycin (Gen), kanamycin (Kan), streptomycin (Str), tetracycline (Tet), minocycline (Min), and chlortetracycline (Chl; Figure 1e). By contrast, the growth of MDR E. coli in culture medium was almost unaffected by MWH or antibiotics at sub-MIC90 levels alone. Meanwhile, Gen could not effectively raise the temperature under MW radiation (Figure S1, Supporting Information), suggesting that the antibacterial MWH was likely generated by MW-driven PLGA MPs only. Compared with the MWH treatment, only a slight increase in CFU was observed when the mixture of Gen at 1/2MIC<sub>90</sub> concentration and bacteria was heated to ≈50 °C in a water bath, which suggests that hyperthermia played a decisive role in reversing AbR (Figure S2, Supporting Information). However, MW is more preferable for clinical practice owing to its powerful tissue penetration and noninvasion.<sup>[29]</sup> To examine the ability of MWH to potentiate the bactericidal activities of antibiotics, the concentration of antibiotics was further reduced. The MIC<sub>90</sub> of  $\beta$ -lactam (Pen, Amo, and Cef) was decreased fourfold in the presence of MWH (Figure 1f; Figure S3a,b, Supporting Information), whereas the MIC<sub>90</sub> of aminoglycoside (Gen, Kan, and Str) and tetracycline (Tet, Min, and Chl) was even reduced at least eightfold (Figure 1g,h; Figure S3c-f,

Supporting Information) in the same condition, indicating that MWH had resensitized MDR *E. coli* to multiple existing clinical antibiotics, thus reversing AbR.

# 2.2. MWH Downregulates BamA Protein Expression and Inhibits BAM Complex Biogenesis

The aforementioned results suggest that MWH might perform a common potentiating mechanism that assists different classes of antibiotics in reversing MDR  $E.\ coli$ . We then used tandem mass tag (TMT), high-performance liquid chromatography (HPLC), and mass-spectrometry-based proteomics to analyze the protein changes in MDR  $E.\ coli$  after MWH treatment. First, a heat map was drawn based on the Pearson correlation coefficients calculated between the pairings of all specimens (Figure S4, Supporting Information), which is a common method used to determine the degree of linear correlation between two sets of data. [30] All correlation coefficients were calculated within the acceptable ranges (|r| > 0.6). Subsequently, 2338 quantifiable proteins were detected by performing a quantitative proteomic study and presented in a volcano plot (Figure 2a), where 34 significantly upregulated

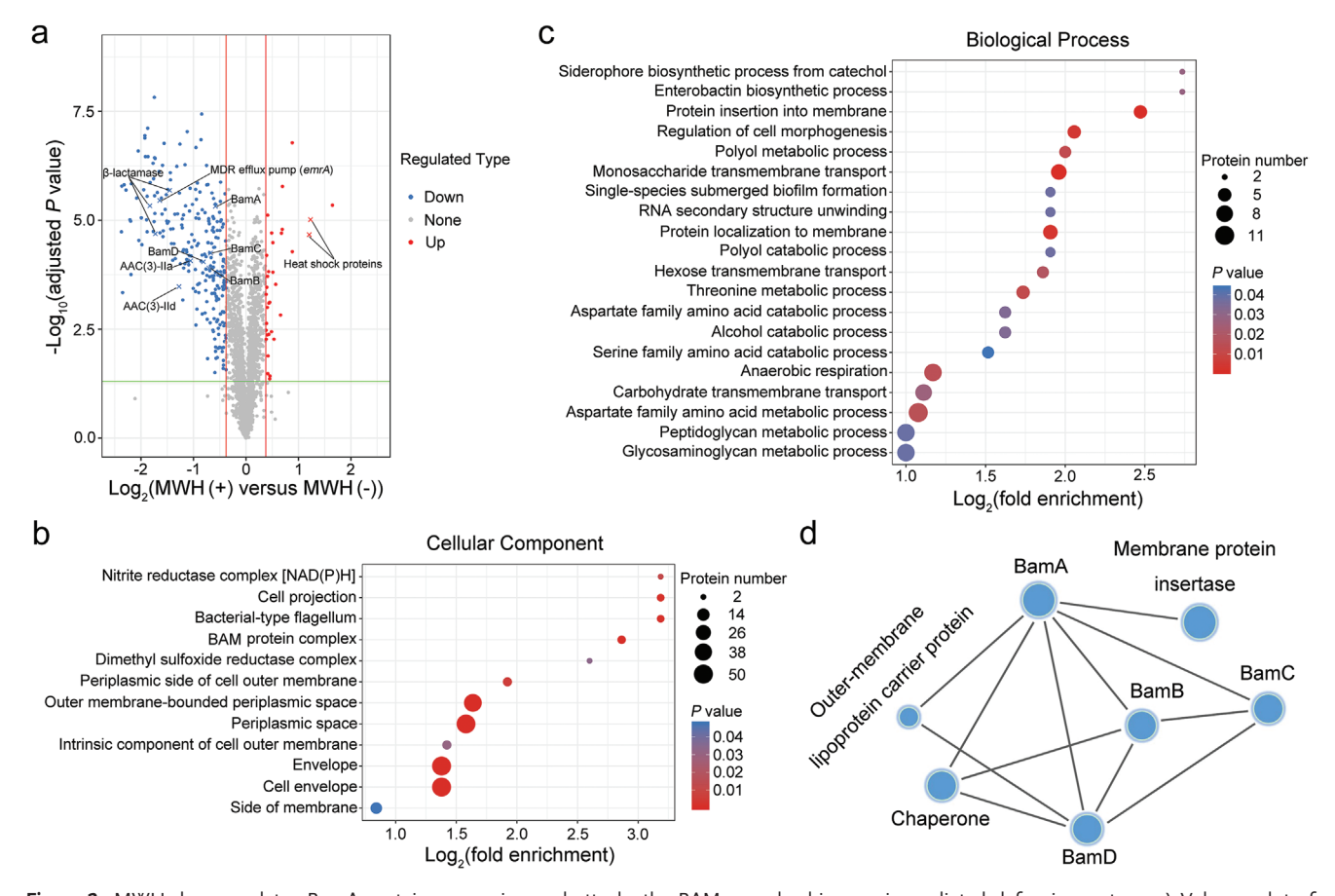


Figure 2. MWH downregulates BamA protein expression and attacks the BAM complex biogenesis-mediated defensive system. a) Volcano plot of the MDR *E. coli* proteomic study of differentially expressed proteins after treatment with (MWH (+)) or without (MWH (-)) MWH. b) Bubble map of downregulated cellular component enrichment in the MDR *E. coli* MWH (+) and MWH (-) groups. c) Bubble map of the top 20 categories with the most significant enrichment in the downregulated biological process in the MDR *E. coli* MWH (+) and MWH (-) groups. d) PPI network analysis of downregulated essential outer membrane protein expressions. Data are taken from independent samples (n = 3).





www.afm-journal.de

proteins (red dots; p < 0.05; with a fold change in expression level of >1.3) and 268 significantly downregulated proteins (blue dots; p < 0.05; with a fold change in expression of <1/1.3) were identified, which suggests a wide range of cellular, biological, and functional changes due to MWH treatment. Moreover, two heat shock proteins were observed to be obviously upregulated, which is a timely response for organisms to survive at febrile temperatures. [31,32]

UniProt annotations further reflected that several downregulated proteins with subcellular localization were specifically enriched in the OM. OMPs, including BamA, BamB, BamC, and BamD proteins, were significantly downregulated by MWH treatment. BamA, the core component in the essential BAM-protein complex, is itself a 16-strand OMP superfamily member that contains a  $\beta$ -barrel domain across the OM (Figure S5, Supporting Information). [33-35] One end of the BamA  $\beta$ -barrel domain extends into the periplasm to scaffold BamB-D, while the other end is exposed extracellularly. Hence, this specific structure turns it to be vulnerable when the bacteria expose to toxic environments. In addition, we found that the clusters of orthologous groups (COG) of up to 31 downregulated proteins mainly affected the biogenesis of the cell wall/ membrane/envelope (Figure S6, Supporting Information). These results show that MWH might act on the OM. We then utilized gene ontology (GO), an important bioinformatic analysis method, to describe the various properties of genes and gene products.<sup>[36]</sup> The biological functions of all the downregulated proteins were typically explained by their cellular components, biological processes, and molecular functions (Figure S7, Supporting Information). Obviously, the cellular components of the membrane and protein-containing complex were enriched with enormous downregulated proteins, which were further divided into the top 20 most significantly enriched categories in more detail by a bubble map (Figure 2b). The downregulated cellular components showed a significant enrichment in the BAM-protein complex, the intrinsic component of the bacterial OM, and the space between the OM and the periplasm where the BamA protein structure spans. These data suggest that the essential changes were related to the downregulation of BamA because it is an insertase and the hub unit in the essential BAM-protein complex to facilitate the insertion and folding of OMPs.[37]

The downregulation of cellular components inevitably impairs the corresponding biological processes. Therefore, we screened out the results of the top 20 categories with the most significant downregulation in the biological process of GO. As expected, protein insertion and localization into membranes were inhibited by the downregulation of BamA expression (Figure 2c). We found that the catabolic and metabolic processes of some amino acids were also blocked, which might be attributed to the consequence of the downregulation of BamA protein expression impairing the ability of the BAM complex to capture and transport the nascent OMPs synthesized by amino acids promptly. To further examine the obstructed mechanisms of transportation, insertion, and folding of OMPs, a protein-protein interaction (PPI) network analysis was performed. BamA-D proteins, the unique components of the BAM complex,[38,39] strongly interacted with each other (Figure 2d), indicating that their close cooperation maintained the regular operation of the BAM complex. The BamA protein was also associated with the membrane protein insertase YidC, OM lipoprotein carrier protein lolA, and survival factor A (SurA) chaperon.

# 2.3. MWH Disorders the BamA Protein Structure and Enhances OM Permeability

As all the changes occurred according to the downregulation of BamA protein expression, we hypothesized that a direct interaction exists between MWH and BamA protein, which was subsequently examined and mapped by molecular dynamic (MD) simulation. We obtained the crystal structure of the BamA protein from the Protein Data Bank code 6FSU and simulated the dynamic changes in the protein structure at 37 and 50 °C for 100 ns, respectively. To simplify the MD simulation, we set 37 °C as the condition without MWH treatment and 50 °C as the condition with MWH treatment. We first extracted the conformation after 100 ns of MD simulation for model analysis. Compared with the structure without MWH treatment (green structure), the BamA protein structure treated with MWH loosened and became more open (blue structure), which had an adverse effect on the stability of the integral structure (Figure 3a). Notably, strong substantial chemical shift perturbations were observed in the extracellular and periplasmic loops of BamA, whereas no conformational changes were observed within the  $\beta$ -barrel domain in the OM space. However, the new antibiotics only induced chemical shift perturbations in the extracellular loop of BamA, [17,18] which suggests that MWH strongly interacted with the BamA protein.

We then analyzed important adverse parameters related to protein structure to shed light on the conformational changes in protein structure in detail. The root mean square deviation (RMSD) was calculated to investigate the fluctuation of the protein backbone in the MD process. The fluctuation of the BamA protein skeleton approached equilibrium after 50 ns with or without MWH treatment. The subsequent fluctuation of the protein skeleton treated with MWH was more remarkable than that treated without MWH (Figure 3b), indicating that the BamA protein backbone was extremely unstable under the MWH treatment. To further locate the fluctuation of the BamA protein backbone, root mean square fluctuation was used to reveal the perturbation of the amino acid residues of the BamA protein. We focused on the fluctuation of amino acid residues at positions 500-800 due to the consideration of BamA protein structure. Positions 670-700 (red-dotted rectangle) showed the most significant fluctuations with MWH treatment (Figure S8, Supporting Information), which corresponded to the chemical shift perturbations of the amino acid residues in the extracellular loops of BamA, including ASP-685, TYR-686, GLY-695, and ALA-696 (Figure 3a). In addition, amino acid residues in the periplasmic loops, including ARG-583, TYR-585, LYS-728, and TYR-729, also showed an obvious fluctuation. We hypothesized that the fluctuation of amino acid residues in this region affects the protein structure and interferes with the PPI function.

The gyrate radius, an important scale parameter, was used to describe the structural stability of proteins. Compared with the non-MWH treatment group, the gyrate radius of the

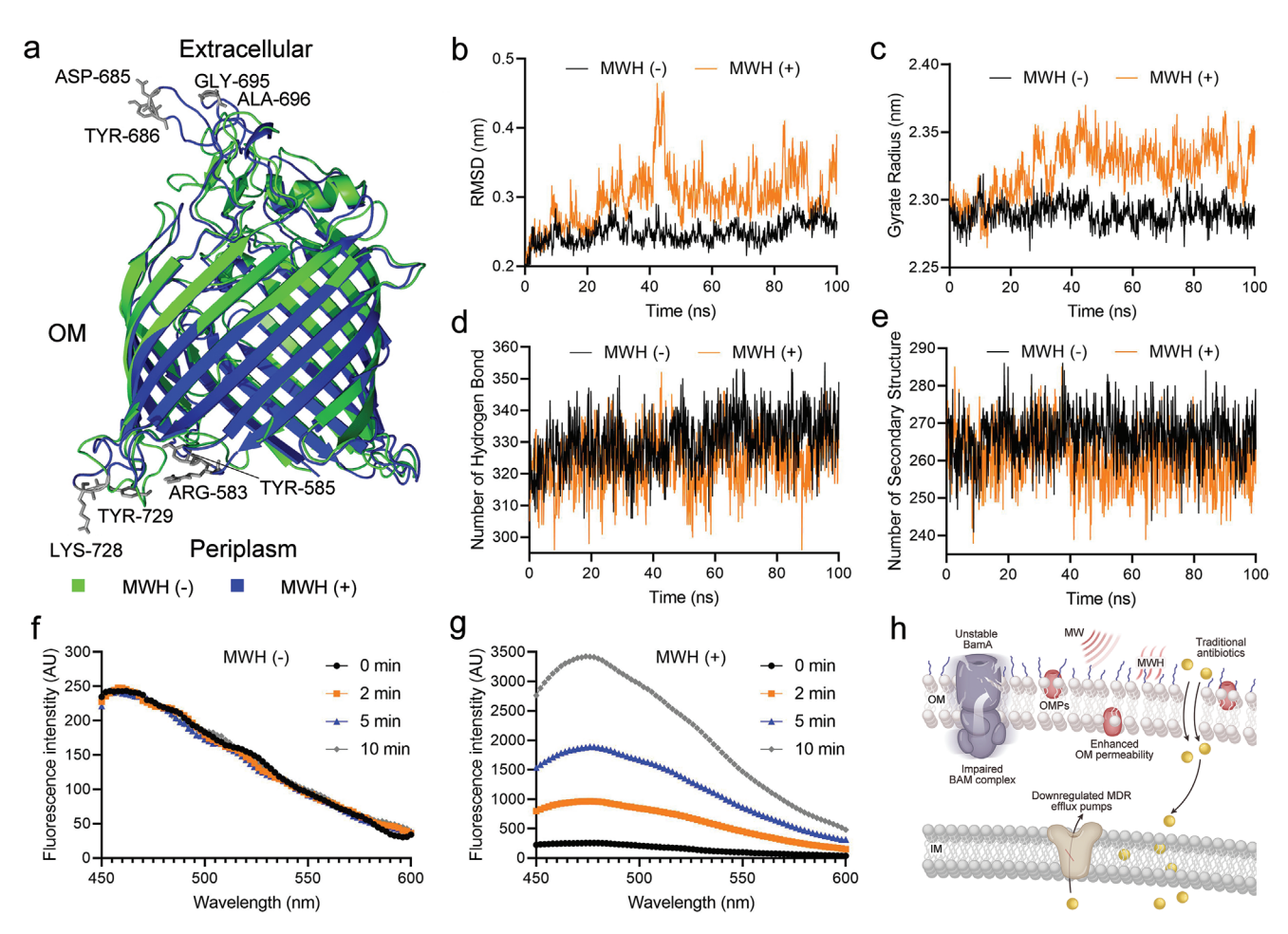


**Figure 3.** MWH destabilizes the BamA protein structure and enhances outer membrane permeability. a) Interactions of MWH on the BamA  $\beta$ -barrel structure. Green: normal BamA  $\beta$ -barrel structure without MWH treatment (MWH (–)). Blue: unstable BamA  $\beta$ -barrel structure with MWH treatment (MWH (+)). Labeled residues (in grey) exhibited substantial chemical shift perturbations after treatment with MWH. Real-time change in b) root mean square deviation (RMSD), c) gyrate radius, d) number of hydrogen bond, and e) number of secondary structures of the BamA  $\beta$ -barrel structure with (MWH (+)) or without MWH treatment (MWH (–)) for 100 ns. OM permeation determined using the ANS fluorescent probe f) without (MWH (–)) or g) with MWH treatment (MWH (+)). h) Representation of the enhancement of OM permeability through the downregulation and turbulence of BamA protein expression and attack on the BAM complex biogenesis and MDR efflux pumps.

BamA protein backbone was significantly increased under MWH treatment (Figure 3c), indicating that MWH treatment resulted in a looser and unstable protein conformation and even impaired the important functions of the BamA protein, including PPI and catalytic activity. Moreover, after the MWH treatment, the average number of hydrogen bonds in the BamA protein decreased from 330 to 323, and the average number of secondary structures was reduced from 267 to 260 (Figure 3d,e). This further suggests that the interaction forces within the protein were decreased, which was not conducive to the overall stability of the BamA protein backbone.

As the BamA protein is strongly associated with the biogenesis of the OMPs spanned in the OM, we therefore hypothesized that the downregulation of BamA protein expression and structural disorders might further disrupt the OM permeability barrier. We subsequently evaluated the OM permeability of MDR *E. coli* using the 8-anilinonapthalene-1-sulfonic acid (ANS) dye. Indeed, ANS is a sensitive probe to emit fluorescence light, when it penetrates to the OM and binds with the

hydrophobic region of the OM. No obvious change was observed in the fluorescence intensity of ANS for 10 min without MWH treatment (Figure 3f), indicating that the permeability of the MDR *E. coli* bacterial OM was not affected. After treatment with MWH, the permeability of the MDR *E. coli* bacterial OM was significantly enhanced with an increase in treatment time by monitoring the enhancement of ANS fluorescence intensity (Figure 3g; Figure S9, Supporting Information). Notably, the OM permeability enhanced by MWH was more than three times stronger than that enhanced by dipeptide molecules.<sup>[40]</sup>

In addition, the downregulation of the MDR efflux pump (EmrA) was also detected (Figure 2a). EmrA, an adapter protein in the periplasm, can effectively transfer and excrete antibiotics that have escaped from OM filtration, thus inducing a further protective effect on MDR *E. coli* from antibiotics.<sup>[41]</sup> In fact, our MWH strategy simultaneously reduced the barrier of the BamA protein-associated OM permeability and impaired the action of the MDR efflux pump, allowing the smooth uptake of antibiotics (Figure 3h).

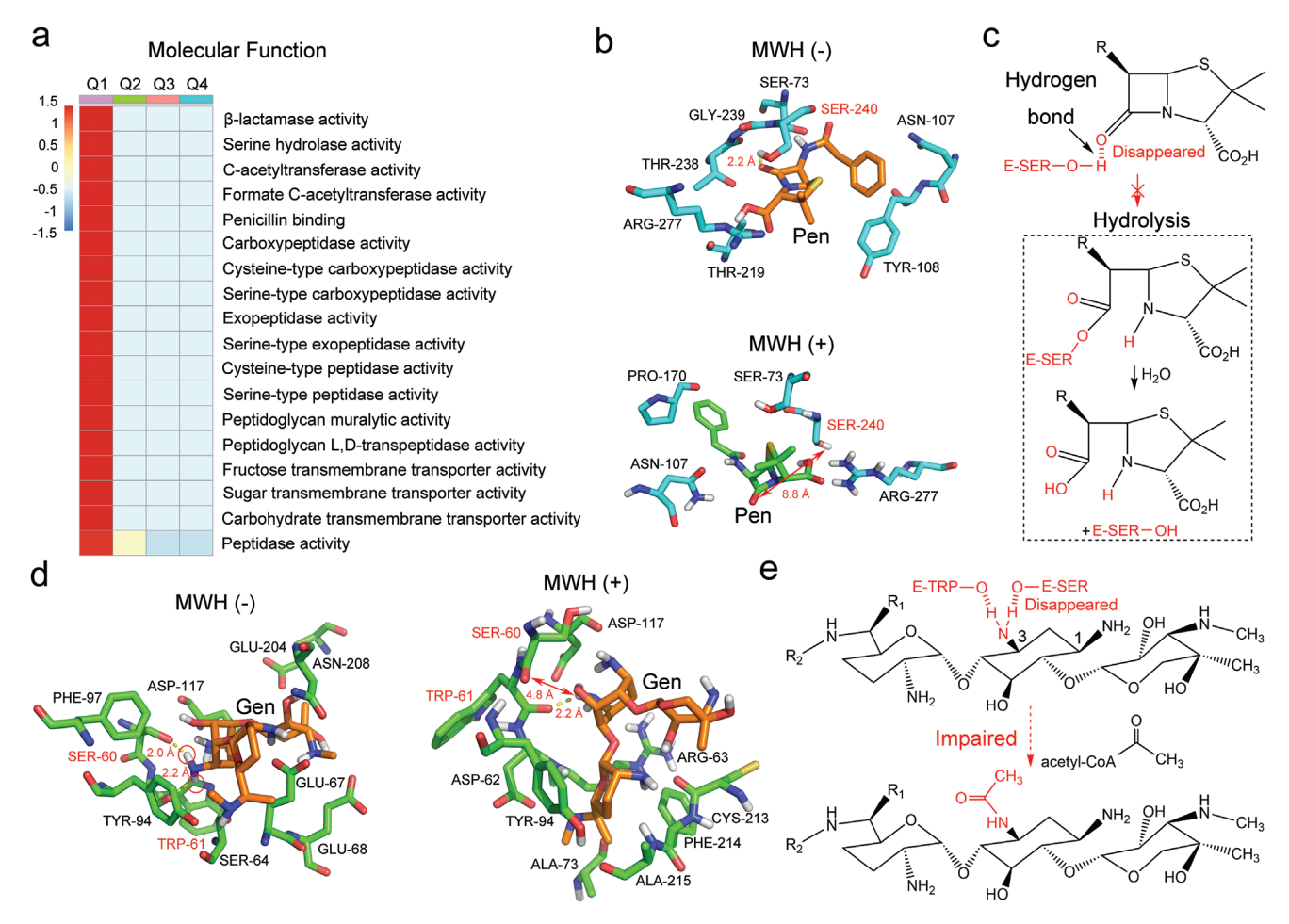


Figure 4. MWH attacks enzymatic degradation or modification-mediated defensive system. a) Heatmap analysis of the differentially expressed molecular function in multidrug-resistant *E. coli* in the MWH (+) and MWH (–) groups. Q1 indicates the most significant downregulation. Red represents strong enrichment, while blue indicates weak enrichment. Data are taken from independent samples (n = 3). b) Interactions of Pen with β-lactamase without (MWH (–)) or with MWH treatment (MWH (+)). The light blue structures on the outside represent the catalytic residues of β-lactamase. The central structure indicates Pen, and the yellow-dotted line indicates a hydrogen bond. c) General hydrolysis mechanism of Pen for β-lactamase and the corresponding mechanism of MWH-induced inhibition. d) Interactions of Gen with aminoglycoside AAC (3)-modifying enzymes without (MWH (–)) or with (MWH (+)) MWH treatment. The green structures on the outside represent the catalytic residues of the AAC (3)-modifying enzyme. The central structure indicates Gen, and the yellow-dotted line indicates a hydrogen bond. e) General modifying mechanism of Gen for the AAC (3)-modifying enzyme and corresponding mechanism of MWH-induced inhibition.

### 2.4. MWH Inhibits Enzymatic Degradation or Modification

The results show that MWH assisted the existing traditional antibiotics in breaking through the most important barrier of OM permeability and the subsequent obstacle of the MDR efflux pump though. The antibiotics would be still confronted with the threat posed by hydrolytic or modifying enzymes before reaching the intracellular space to realize their bactericidal effects. Hopefully, we identify that the downregulation of the related  $\beta$ -lactamase and aminoglycoside N(3)-acetyltransferase ([AAC (3)]; a modifying enzyme) was detected (Figure 2a). In a subsequent quantitative proteomic analysis, we divided the differentially expressed proteins into four parts (Q1–Q4) according to their differentially expressed multiples. The 192 most significantly downregulated proteins were classified into the Q1 category (Figure S10, Supporting Information). According to the Fisher exact test p

value, we used the hierarchical clustering method to gather the relevant molecular functions of GO to develop a heat map, where red represented strong enrichment and blue indicated weak enrichment (**Figure 4**a). Interestingly, the activities of  $\beta$ -lactamase and acetyltransferase were significantly enriched in the Q1 category, indicating that the expression of the hydrolytic and modifying enzymes was not only downregulated, but their catalytic activities were also severely inhibited by MWH treatment.

To better understand the molecular mechanisms of MWH-induced inhibition, we performed a MD simulation and obtained the high-resolution X-ray structures of antibiotics and associated enzymes. In the typical enzymatic process, traditional  $\beta$ -lactam antibiotics are usually hydrolyzed by  $\beta$ -lactamase, while aminoglycoside antibiotics are modified by modifying enzymes. [42–44] Therefore, in the simulation process, representative Pen and Gen were used for



FUNCTIONAL FUNCTIONAL

www.afm-journal.de

molecular docking with  $\beta$ -lactamase and AAC (3), respectively. Pen was observed to interact mainly with the amino acid residues SER73, SER240, ASN107, TYR108, THR219, ARG277, THR238, and GLY239 of the  $\beta$ -lactamase noncovalently without MWH treatment (Figure 4b). Notably, the distance between the oxygen group (-O) of Pen and the hydroxyl group (-OH) of SER240 was only 2.2 Å, and a strong hydrogen bond (indicated as yellow-dotted line) between them was formed, which plays a crucial role in hydrolvsis. [45,46] The positively charged residues on  $\beta$ -lactamase (indicated as E-SER-OH) first attracted a negatively charged carboxylate on the azetidinone ring of Pen, resulting in the formation of a key hydrogen bond between the -O of Pen and the -OH of serine (SER) on  $\beta$ -lactamase, where acylation immediately occurred (Figure 4c). Subsequently, water molecules entered the system and activated deacylation that resulted to the opening of the ring and then inactivated microbiological Pen. However, we observed that the hydrogen bond disappeared due to the increased distance between the -O of Pen and the -OH of SER240 from 2.2 to 8.8 Å after treatment with MWH (Figure 4b). Thus, this indicated that the subsequent acylation and deacylation of the hydrolysis process were inhibited by MWH treatment, which in turn protected the  $\beta$ -lactam antibiotics from the hydrolysation by  $\beta$ -lactamase. In addition, by suppressing the activity of penicillin-binding proteins (PBPs),  $\beta$ -lactam antibiotics can inhibit the synthesis of peptidoglycan, a critical component of the bacterial cell wall, which eventually inhibits cell wall synthesis.<sup>[47,48]</sup> We observed that the penicillin-binding ability and activity of peptidases belonging to PBPs were impaired, further impeding the metabolic activities of cell wall-related peptidoglycan synthesis and transmembrane transport (Figures 2c,4a). This finding demonstrates that MWH not only kept the  $\beta$ -lactam antibiotics away from the threat of  $\beta$ -lactamase but also synergized with  $\beta$ -lactam antibiotics to inhibit bacterial cell wall synthesis for bactericidal purposes.

We observed that similarly to  $\beta$ -lactamase, the amino acid residues GLU204, ASN208, GLU67, GLU68, SER64, TRP61, TYR94, SER60, PHE97, and ASP117 on the AAC (3)-modifying enzyme interacted with Gen when the MWH treatment was absent (Figure 4d). Key hydrogen bonds (indicated as yellow-dotted lines) were also formed between the residues (SER60 and TRP61) and the hydrogen atom (indicated as a red circle) of the amino group (-NH<sub>2</sub>) at position 3 on Gen. This enhanced the ability of the AAC (3) to target Gen and impair the bactericidal function of this kind of antibiotic. In the process of modification, AAC (3) mainly acted on the hydrogen atom of -NH2 on Gen at position 3, resulting in the formation of key hydrogen bonds between the hydrogen atom of -NH2 and the oxygen atom of AAC (3) residues (indicated as E-TRP-O and E-SER-O). Subsequently, -NH<sub>2</sub> is deprotonated and amidated in the presence of acetyl-coA, which leads to the inactivation of Gen.<sup>[49,50]</sup> However, the hydrogen bond between the hydrogen atom of -NH2 and the oxygen atom of the SER60 residue disappeared as the increased distance between them was found from 2.0 to 4.8 Å after treatment with MWH (Figure 4d). This change weakened the catalytic process owing to the impairment of subsequent deprotonation and amidation (Figure 4e).

# 2.5. Gen-PLGA MPs Potentiate the Bactericidal Effects on MDR E. Coli-Associated UTI and PI

To verify the clinical feasibility of MWH system, we next loaded Gen into PLGA MPs using the water-oil-water double emulsion evaporation method to obtain Gen-PLGA MPs. PLGA and Gen-PLGA MPs were uniformly dispersed in saline and were then observed under a microscope (Figure 5a,b). We generated PLGA MPs with a uniform size of ≈20 µm. The size of PLGA MPs was increased to 30-40 µm after loading Gen. Interestingly, the natural spherical structure of PLGA or Gen-PLGA MPs collapsed and reassembled into a supersized sheet structure after MW irradiation. The same collapse process occurred in the Pen- (Pen-PLGA MPs) and Tet-loaded PLGA MPs (Tet-PLGA MPs; Figure S11, Supporting Information). We hypothesized that the mechanism of the MW thermal response involved the activation and motion of PLGA polymer chain segments under the action of MW mechanical energy (Figure 5c). The motion of PLGA polymeric segments not only converted kinetic energy into heat based on the law of energy conservation but also promoted the transition of PLGA from a glassy state to a highly elastic state. The temperature eventually exceeded the glass transition temperature (44-48 °C) of the PLGA used, causing the entire molecular chain to move and exhibit viscous flow properties. Taken together, the motion of the PLGA molecular chain segments under MW mechanical energy released heat and led to the collapse of the PLGA MPs due to the phase transition mechanism.

We then tested the release of Gen from the PLGA MPs owing to the collapse of the MPs. The loading and encapsulation efficiencies of the Gen-PLGA MPs were 9.54% (Figure 5d) and 85.98% (Figure S12, Supporting Information), respectively. After applied MWH to the Gen-PLGA MPs saline solution for 10 min, we found that 48.79% of Gen was released from the Gen-PLGA MPs. This further confirmed that the PLGA MPs gradually collapsed under MW irradiation. In the in vitro antibacterial tests, Gen-PLGA MPs showed a  $4\log_{10}$  reduction in CFUs against MDR  $E.\ coli$  under MWH treatment (Figure 5e), which was comparable with the antibacterial efficiency of Gen (the same amount of released dose,  $\approx$ 0.186 mg mL $^{-1}$ ) under MWH treatment.

The biocompatibility of the PLGA MPs and Gen-PLGA MPs was evaluated by using cytotoxicity and hemolysis assays. We found that both of the PLGA and Gen-PLGA MPs demonstrated comparable biocompatibility to fibroblasts (Figure S13, Supporting Information). Also, neither PLGA nor N PLGA MPs would induce any hemolysis in red blood cells (RBCs) (Figure S14, Supporting Information). To demonstrate the efficacy of PLGA MPs-induced MWH to reverse AbR in vivo, we proposed to use two MDR E. coli UTI and PI models to highlight how the restoration of sensitivity to Gen could be achieved by our strategy in deep tissue infections, respectively. In the UTI model, the rats were inoculated with ≈10<sup>6</sup> CFU MDR E. coli via a catheter inserted in the urethra into the bladder. At 1 h after infection, the rats were injected with saline, Gen, PLGA MPs, and Gen-PLGA MPs using the same method and immediately treated with MW. The skin temperature of the saline group only increased to 39.7 °C after 10 min of MWH treatment (Figure 6a). The Gen plus MW group was also unable to

www.afm-journal.de

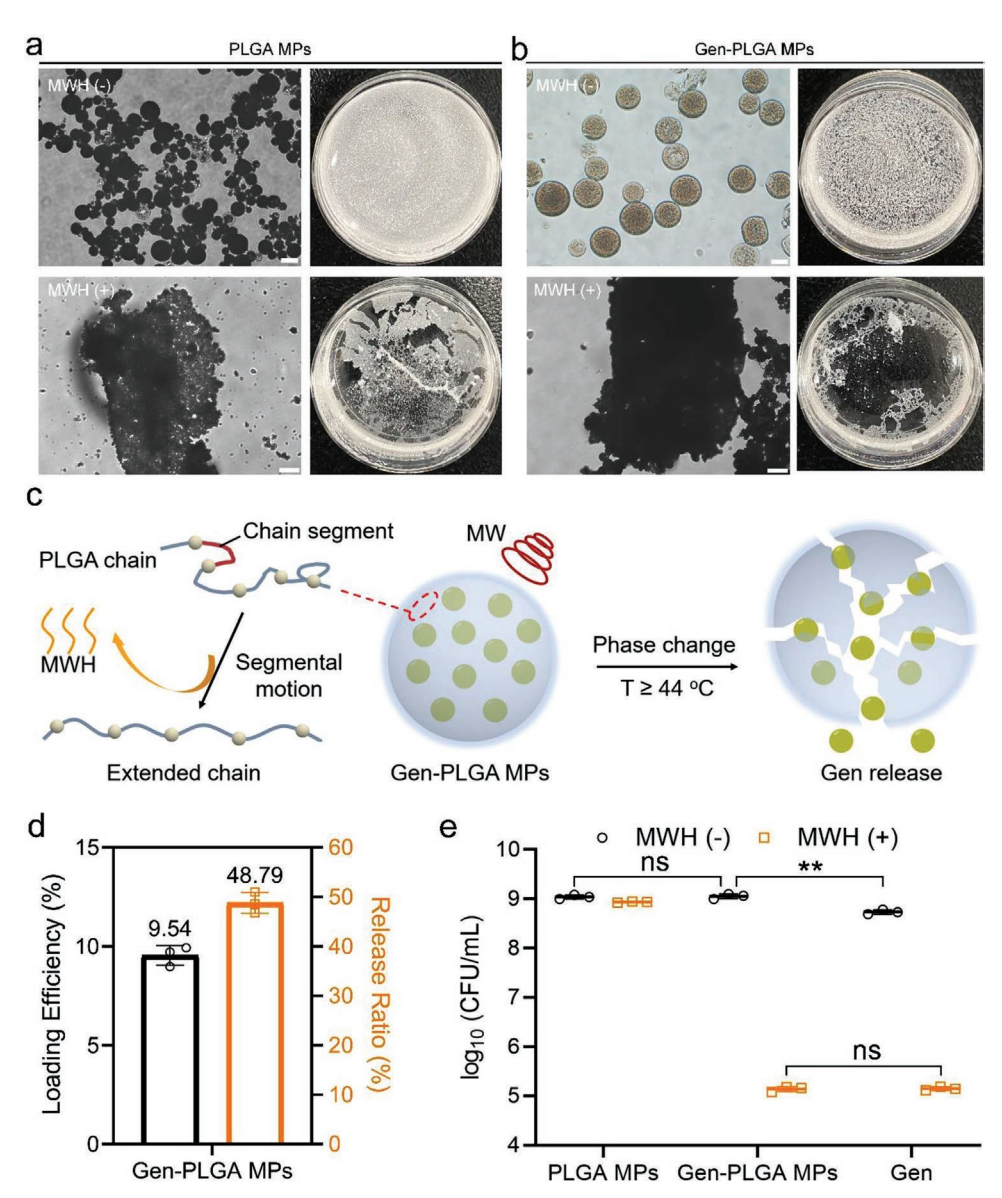


Figure 5. PLGA MPs load and release Gen. The morphologies (left) and dispersion conditions (right) of a) PLGA MPs and b) Gen-PLGA MPs without (MWH (-)) or with MWH treatment (MWH (+)). Scale bar: 20  $\mu$ m. c) Representation of PLGA MP-induced MWH and Gen release under MW irradiation. d) The loading efficiency of Gen in Gen-PLGA MPs and the release ratio of Gen from Gen-PLGA MPs after 10 min of MW irradiation. e) PLGA MPs, Gen-PLGA MPs, and Gen (the same amount of released dose,  $\approx$ 0.186 mg mL<sup>-1</sup>) against MDR *E. coli* without (MWH (-)) or with MWH treatment (MWH (+)) for 10 min. Data are taken from independent samples (n = 3). The error bars indicate mean  $\pm$  standard deviation: \*p < 0.05, \*\*p < 0.01, \*\*\*\*p < 0.001; ns: not significant (p > 0.05). The statistical analysis was performed using a two-sample Student t-test.

respond to the MWH therapy owing to the negligible thermal response of Gen to MW (Figure S15a, Supporting Information). In contrast, PLGA or Gen-PLGA MPs in the bladders were rapidly excited and released heat due to the powerful tissue penetration of MW. The skin temperature was subsequently detected to be >48 °C after 10 min of MW treatment in the PLGA and Gen-PLGA MPs treatment groups. The rats were euthanized to assess the MDR *E. coli* bacterial burden in urine, bladders, and kidneys 24 h after treatment. The bacterial burden in urine, bladders, and kidneys did not change significantly in response to Gen or PLGA MPs-induced MWH administered separately (Figure 6b–d). Additionally, there was no significant therapeutic effect in pure Gen group even under

the irradiation of MW (Figure S15b–d, Supporting Information). However, a significant deduction (a 2- to 4-log<sub>10</sub> reduction in CFU) in the MDR *E. coli* bacterial burden was observed in the Gen-PLGA MPs-treated group with the combination of Gen and MWH. Haematoxylin and eosin (H&E) staining was then used to evaluate the therapeutic effects of the MWH system. Many inflammatory cells (indicated by red-dotted circles) appeared and accumulated in the bladders (Figure 6e) and kidneys (Figure S16, Supporting Information) of the rats in the saline, Gen, and PLGA MPs groups because of severe MDR *E. coli* bacterial infection and inflammation. Interestingly, almost no inflammation was present in the bladders and kidneys of the rats in the group treated with Gen-PLGA MPs

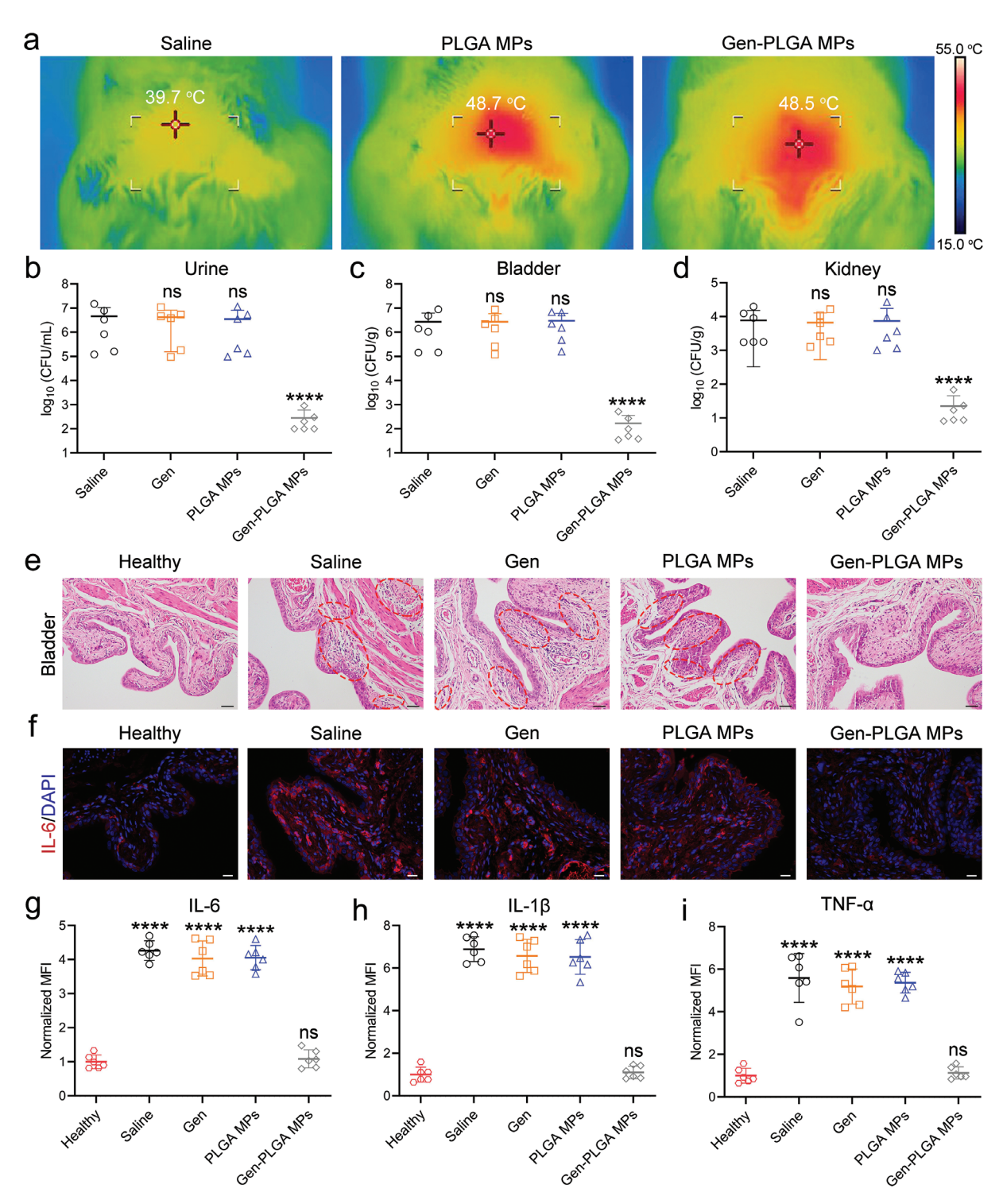


Figure 6. Gen-PLGA MPs potentiate the bactericidal effects in a MDR *E. coli* urinary tract infection model. a) Thermal images at the bladder after injection with saline, PLGA MPs, and Gen-PLGA MPs, and MW irradiation for 10 min. MDR *E. coli* bacterial burden in b) urine, c) the bladders, and d) the kidneys after different treatments. Data were taken from independent samples (n = 6). The error bars indicate mean ± standard deviation: \*p < 0.05, \*\*p < 0.01, \*\*\*p < 0.001, and \*\*\*\*p < 0.0001; ns: not significant (p > 0.05). Statistical analysis was performed using a two-sample Student t-test. e) Haematoxylin and eosin staining images of the harvested bladders after different treatments. Scale bar: 50 μm. The red-dotted circles indicate inflammatory cells. f) Representative images of immunofluorescence staining of IL-6 in the harvested bladders after different treatments, obtained at an original magnification of 40×. Scale bar: 20 μm. Quantification of the mean fluorescence intensity (MFI) normalized to the mean "Healthy" g) IL-6, h) IL-1 $\beta$ , and i) TNF- $\alpha$ , as indicated in (f), Figures S17,S18, Supporting Information, respectively. Data were obtained from independent samples (n = 6). The error bars indicate mean ± standard deviations: \*p < 0.05, \*\*p < 0.05, \*\*p < 0.01, \*\*\*p < 0.001, and \*\*\*\*p < 0.0001; ns: not significant (p > 0.05). The statistical analysis was performed using one-way analysis of variance with the Tukey multiple-comparisons test.





www.afm-journal.de

with the combination of Gen and MWH, indicating that MWH effectively resensitized MDR E. coli to Gen. Notably, compared with healthy bladders and kidneys, tissues showed no obvious changes or lesions after MWH treatment (Figure 6e; Figure S16, Supporting Information), which suggests that our MWH is a biosafe therapeutic technique and has great potential for further clinical practice. To further examine the infection-related inflammatory response in the tissues, immunofluorescence staining was applied to evaluate the level of proinflammatory cytokines, including interleukin-6 (IL-6), interleukin-1 beta (IL-1 $\beta$ ), and tumor necrosis factor-alpha (TNF- $\alpha$ ). Compared with the healthy group, IL-6 (Figure 6f), IL-1 $\beta$  (Figure S17, Supporting Information), and TNF- $\alpha$ (Figure S18, Supporting Information) were strongly expressed in the bladders of the rats in the saline, Gen, and PLGA MPs groups. Quantification of the normalized mean fluorescence intensity (MFI) of IL-6 (Figure 6g), IL-1 $\beta$  (Figure 6h), and TNF- $\alpha$  (Figure 6i) further reflected severe inflammation in the groups, which showed no bactericidal ability. However, no significant difference in terms of inflammatory response was found between the healthy bladders and the Gen-PLGA MPs-treated bladder. We also observed a strong inflammatory response in the kidneys of the rats in the saline, Gen, and PLGA MPs groups (Figure S19, Supporting Information). But no significant difference was found between the healthy and Gen-PLGA MPs-treated kidneys.

In the PI model, excellent MWH properties were observed in the PLGA and Gen-PLGA MPs (Figure S20, Supporting Information). The Gen-PLGA MPs effectively eliminated MDR  $E.\ coli$  in peritoneal fluid owing to the rapid release of MWH and Gen (Figure S21, Supporting Information). However, MWH or Gen alone was ineffective against MDR  $E.\ coli$ , which led to severe PI and the accumulation of considerable inflammatory cells in the peritonea (Figure S22, Supporting Information). Similarly, IL-1 $\beta$  (Figure S23, Supporting Information) and TNF- $\alpha$  (Figure S24, Supporting Information) inflammatory cytokines were strongly expressed in the peritonea of the rats in the saline, Gen, and PLGA MPs groups. However, no significant difference was found between the healthy peritoneums and Gen-PLGA MPs-treated peritonea in terms of tissue morphology and inflammatory response.

# 3. Discussion

In this study, we developed an effective strategy of re-sensitizing the existing conventional antibiotics by disabling the general defense mechanisms of MDR Gram-negative bacteria: the BAM complex biogenesis system, MDR efflux pump system, and enzymatic degradation or modification system. We first demonstrated that MWH potentiated the bactericidal effects of conventional antibiotics, thus reversing the AbR of MDR *E. coli*.

Our data indicate that MWH downregulated BamA protein expression, which is an essential component of the BAM-protein complex.<sup>[51]</sup> The downregulation led to the suppression of the biogenesis of the BAM complex and the transportation, insertion, and folding of the OMPs that the BAM complex manipulated, resulting in an increase in OM permeability and

the promotion of antibiotic uptake subsequently. The PPI network analysis further revealed a relationship between BamA protein expression and OMPs. BamA-D proteins are unique components of the BAM complex.[38,39] In the PPI network, the strong interaction and cooperation among the BamA-D proteins maintained the regular operation of the BAM complex. It was worth noting that the BamA protein was the center of PPI network and its association with the membrane protein insertase YidC, OM lipoprotein carrier protein lolA, and survival factor A (SurA) chaperon manipulated the biological process of OMPs.[33,37] Taken together, these results denote that MWH downregulated BamA protein expression, which in turn interfered with the regular operation of the BAM complex. In fact, the BamA protein expression becomes a concern when new antibiotics targeting MDR Gram-negative bacteria are developed. For instance, the small molecule MRL-494, chimeric peptidomimetic antibiotics, darobactin, and the monoclonal antibody MAB1 were developed to eliminate MDR Gram-negative pathogens that targeted to the BamA protein and disordered its structure.[17-20] Therefore, further examination of the changes in the BamA protein structure of MDR E. coli after treatment with MWH would be interesting.

The present study demonstrated that the MWH attack resulted in temporary structural instability of the BamA protein and substantial chemical shift perturbations in the extracellular and periplasmic loops of the BamA protein. By contrast, the new antibiotics only induced chemical shift perturbations in the extracellular loop, [17,18] which suggests that the MWH attack substantially weakened the BamA protein expression. As a result, OM permeability was significantly enhanced three times more than that induced by dipeptide molecules.[40] Our study demonstrates that the BamA protein as the core component of the BAM complex could manipulate OMP biogenesis and OM permeability. The application of MWH could therefore impair the intracellular components and biosynthesis of OM through the downregulation of BamA protein expression. Hence, its structural integrity was compromised and ultimately weakened the MDR E. coli bacterial OM permeability barrier.

We also observed that MWH impaired the function of the MDR efflux pump by downregulating the expression of its related protein (EmrA),<sup>[41]</sup> which was supposed to transfer and excrete antibiotics from OM filtration.<sup>[52]</sup> However, further study will be necessary to determine how the downregulation of EmrA protein causes downstream impairment of MDR efflux pump. Previous work has demonstrated that the EmrA adapter protein has been linked to OM channel TolC, which formed part of a number of efflux systems in MDR *E. coli*.<sup>[41]</sup> One possibility is that the interaction of MWH with EmrA prevents TolC function by disrupting essential conformational changes of EmrA.

To revitalize the effectiveness of conventional antibiotics on MDR *E. coli*, another powerful defense system at the cellular level, which is enzymatic degradation or modification system, [42–44] in addition to the OM permeability barrier and MDR efflux pump, must be considered. Surprisingly, MWH not only inhibited the synthesis of the hydrolytic and modifying enzymes but also suppressed the enzyme catalytic process through the inhibition of the key hydrogen bond formation between the catalytic residues of enzymes and the corresponding functional groups of antibiotics.



www.afm-journal.de

ADVANCED FUNCTIONAL MATERIALS

Our study demonstrated that MWH was able to potentiate the efficacy of a wide variety of conventional antibiotics against MDR *E. coli*. This approach could completely paralyze the defense systems established by bacteria that coped with antibiotic stress. The literatures reported that the re-establishment of those bacterial defense systems required a long-term evolution brought by clinically dedicated AbR genes.<sup>[53,54]</sup> In contrast, our MWH treatment on MDR *E. coli* bacteria only lasted for 10 min. Therefore, we speculated that the genetic evolution of MDR *E. coli* bacteria would unlikely develop any new AbR in such short period of time. However, this hypothesis has to be tested by further experiments.

Another notable outcome was the drug release mechanism of PLGA MPs induced by MWH. The mechanical energy induced by MW excited the motion of PLGA polymer chain segments, contributing to the conversion of kinetic energy into thermal energy according to the law of energy conservation. The vibration of the PLGA polymeric segments promoted the transition of PLGA from a glassy state to a highly elastic state. Owing to this phase transition, the PLGA MPs collapsed, thereby releasing antibiotics. As the glass transition temperature of the PLGA polymer was maintained at 44 to 48 °C in our experiments, the entire PLGA molecular chain started to vibrate when the temperature just exceeded its glass transition temperature. Eventually, the PLGA polymer exhibited viscous flow properties that led to the collapse of PLGA MPs; therefore, the antibiotics were released.

Our MWH strategy demonstrated high treatment effectiveness to reduce the bacterial burden in urine and infected bladders and kidneys compared with treatment with new peptide-based antibiotics in the MDR *E. coli* UTI model.<sup>[55]</sup> For instance, the new peptide antibiotic only reduced 2-log<sub>10</sub> of *E. coli* in the infected bladders after 3 days of treatment,<sup>[55]</sup> while our MWH plus conventional antibiotic therapeutic strategy exhibited a 4-log<sub>10</sub> reduction in bacterial burden in the urine and bladders after a short treatment period. In addition, MW-responsive multifunctional Gen-PLGA MPs also demonstrated robust antibacterial activities in PI without causing significant inflammation, which further suggests that our MWH therapy is clinically feasible and highly effective for the treatment of deep tissue infections.

## 4. Conclusion

In summary, the proof-of-concept results suggested a new approach to reverse the AbR of MDR Gram-negative bacteria by simultaneously disabling their general defense systems, resulting in higher intracellular drug accumulation and bacterial death subsequently. The combination of defense system inhibitors and conventional antibiotic interventions proved to be a powerful tool against pathogens with high levels of resistance (even >8 mg mL $^{-1}$ ). Moreover, the combined approach drastically reduced antibiotic dosages, thereby reducing harmful side effects while maintaining the same antibacterial activity. In addition, MWH, a defense system inhibitor, in combination with traditional antibiotics had high potential to reduce the emergence and spread of AbR.

#### 5. Experimental Section

Materials: PLGA (RESOMER RG 503 H) was purchased from Sigma Aldrich (St Louis, MO, USA). Dichloromethane (DCM) was purchased from Sinopharm Chemical Reagent Co., Ltd. (Beijing, China). Poly(vinyl alcohol) (PVA), ANS, and antibiotics were bought from Aladdin Regents Co., Ltd (Shanghai, China). The bacterial strain *E. coli* EPEC (BNCC 186732) was bought from BeNa Culture Colletion Co., Ltd (Beijing, China).

Preparation of PLGA MPs: PLGA MPs were obtained using an oil-inwater double emulsion evaporation method. Briefly, PLGA (200 mg) was thoroughly dissolved in 7 mL of DCM solution, and 30 mg of Gen was dissolved in 375  $\mu L$  of deionized water. Then, the Gen solution was slowly added to the PLGA solution under continuous stirring. After emulsification, the mixed solution was homogenized (3000 rpm, 2 min) and then blended with 50 mL of 1% PVA solution. After homogenizing for 2 min, the mixture was slowly added to 100 mL of 1% PVA solution, and the DCM was evaporated for 12 h under mild stirring. The obtained Gen-PLGA MPs were washed with deionized water several times and freeze dried for 16 h. Meanwhile, pure PLGA MPs were prepared without the addition of a Gen solution.

Drug Loading Efficiency, Encapsulation Efficiency, and Drug Release of Gen-PLGA MPs: To determine the Gen-loading and encapsulation efficiencies, the supernatant was collected for Gen concentration analysis after the Gen-PLGA MPs were prepared. The Gen-loading and encapsulation efficiencies were defined as follows:

Loading efficiency (%) = 
$$(W_T - W_S) \times 100 / W_{MPS}$$
 (1)

Encapsulation efficiency (%) = 
$$(W_T - W_S) \times 100/W_T$$
 (2)

where  $W_T$  is the total weight of Gen fed, and  $W_S$  is the weight of Gen in the supernatant, while  $W_{MPS}$  is the weight of Gen-PLGA MPs.

To evaluate the Gen release from the Gen-PLGA MPs treated with MWH, 4 mg of Gen-PLGA MPs were dispersed in 1-mL normal saline. The mixture was then radiated with a MW physiotherapy probe (4 W, 50% duty cycle) for 10 min. The supernatant was finally collected for Gen concentration analysis.

All the Gen concentration analyses were performed using a microplate reader (SpectraMax I3MD USA) at 333 nm. Briefly, 2.5 g of o-phthaldialdehyde (OPTA) was first dissolved in 62.5 mL of methanol. Then, 3 mL of 2-mercaptoalcohol and 560 mL of 0.04 M disodium tetraborate were added to the mixture in this order and refrigerated for at least 24 h to obtain an OPTA reagent. The OPTA reagent was mixed with isopropanol at a ratio of 1:4 before use. The Gen solution was mixed 1:1 with the OPTA reagent and incubated for 30 min to obtain Gen-OPTA complexes that were spectrophotometrically detected at 333 nm. The standard curve equation used was as follows:

$$Y = 4.203X + 0.256(R^2 = 0.967)$$
(3)

where X represents the Gen concentration (mg mL<sup>-1</sup>), while Y indicates the absorbance of the Gen concentration at 333 nm.

Microwave Hyperthermal Test: Pure PLGA MPs (4 mg) or Gen-PLGA MPs (4 mg) were dispersed in 1 mL of normal saline, and the suspension was transferred to a 2-mL EP tube. The EP tube was horizontally laid on a MW physiotherapy probe (4 W, 50% duty cycle), and the temperature was measured every 30 s using a thermal imaging instrument.

Determination of the Minimal Inhibitory Concentration ( $MIC_{90}$ ): The CLSI broth microdilution method was used for the determination of  $MIC_{90}$ , which was defined as the MIC of the antibiotics that inhibited the growth of 90% bacteria. MDR *E. coli* (5 × 10<sup>5</sup> CFU in Luria-Bertani [LB] broth) was cultured with different antibiotics in 96-well microtiter plates. The antibiotic concentrations ranged from 0.008 to 16 mg mL<sup>-1</sup>.

Antibacterial Test: Pure PLGA MPs (4 mg) and different antibiotics were dispersed in 1 mL of LB broth containing  $5 \times 10^5$  CFU *E. coli*. The final concentration of the antibiotics was 1/2MIC<sub>90</sub>. The suspension was then treated with or without MW irradiation for 10 min using the MW





www.afm-journal.de

physiotherapy probe (4 W, 50% duty cycle). After that, the suspension was incubated at 37  $^{\circ}$ C for 24 h on a rotary shaker. The concentration of viable bacteria in suspension was analyzed using the plate-coating method. To examine the efficiency of MW heating in combating bacterial drug resistance, experiments were conducted by reducing the final concentration of antibiotics to 1/4MIC<sub>90</sub>, 1/8MIC<sub>90</sub>, 1/16MIC<sub>90</sub>, and 1/32MIC<sub>90</sub>, respectively. To further investigate the capacity of Gen-PLGA MPs in combating bacterial drug resistance, Gen-PLGA MPs with Gen concentrations <1/2MIC<sub>90</sub> were used to perform the antibacterial test.

Proteomic Study: a) Protein extraction: The MDR *E. coli* samples stored at -80 °C were placed in a pre-cooled mortar and ground into powder with the addition of liquid nitrogen. Then, the powder was treated with lysis buffer supplemented with 8 M urea and 1% protease inhibitor under sonication. After centrifugation for 10 min (12 000 ×g, 4 °C), the supernatant was extracted for determination of the protein concentration using a BCA protein assay kit.

- b) Trypsin hydrolysis: Protein samples were incubated with 20% trichloroacetic acid (TCA) at 4 °C for 2 h to generate precipitates. After centrifuging at 4500 ×g for 5 min, the supernatant was abandoned, and the precipitate was washed with acetone three times. The precipitate was airdried and dispersed with 200 mm tetraethylammonium perchlorate under sonication. Trypsin was then added to the mixture with a trypsin-to-protein ratio of 1:50. After enzymolysis for 24 h, the sample was reduced with 5 mm dithiothreitol at 56 °C for 30 min. Finally, the sample was incubated with 11 mm iodoacetamide at room temperature for 15 min in the dark.
- c) TMT labeling: Peptide samples were desalted using Strata-X C18 (Phenomenex, Torrance, CA, USA) and lyophilized. For TMT labeling, 0.5 M TEAB was used to dissolve the peptide, and labeling was performed in accordance with the protocols of the TMT assay kit.
- d) HPLC fractionation: Peptide samples were fractionated using high pH reversed-phase HPLC. Briefly, the samples were loaded into an Agilent 300Extend C18 column (5  $\mu m,\ 4.5\times150$  mm) and eluted with a gradient of 8–32% acetonitrile (pH 9) for 60 min to separate 60 components. The components were merged into nine fractions and lyophilized for further use.
- e) Liquid chromatography-tandem mass spectrometry analysis: Peptide fractions were dissolved with solvent A (0.1% formic acid + 2% acetonitrile) and loaded into an EASY-nLC 1200 UPLC system for separation using four gradient segments (8-25% solvent B [0.1% formic acid + 90% acetonitrile] for 26 min, 25-35% solvent B for 8 min, 35-80% solvent B for 3 min, and 80% solvent B for 3 min), with a flow rate of 450 nL min<sup>-1</sup>. After separation, the peptide fractions were infused into a nanospray ionization (NSI) source for ionization and then subjected to Q Exactive HF-X mass spectrometry (Thermo Fisher Scientific, Waltham, MA, USA) for analysis. The electrospray voltage of the NSI source was 2 kV. Intact peptide ions and the second-order fragments were detected in Orbitrap (Thermo Scientific) with a high resolution of 70 000. The MS1 precursors were scanned from 400 to 1600 m/z with a resolution of 120 000, and the MS2 precursors were scanned under 100 m/z with a resolution of 15 000. Data-dependent acquisition was adopted for data collection, through which 25 peptide ions with the highest signal intensities successively entered the HCD collision cell to be fractured by 28% collision energy. To improve efficiency, the automatic gain control target was set at 50 000, and the max injection time was 50 ms. The dynamic exclusion time was set at 30 s to avoid repeated scanning.
- f) Database search: MS/MS data were retrieved using the MaxQuant 1.5.2.8 search engine and searched against the ZA035TQ database (16876 sequences). This database was supplemented with a reverse decoy database to calculate the false discovery rate (FDR) and a database of known contaminant proteins. For searching and identification, trypsin/P was set as the cleavage enzyme, with a maximum of two missing cleavages allowed. The minimum length and maximum modification number of the peptide fragments were set as 7 amino acid residues and 5, respectively. The mass tolerance of the peptide precursor was 10 ppm for the first search and 5 ppm for the main search. The mass tolerance of the fragment ion was 0.02 Da. Carbamidomethyl (Cys) was included as a fixed modification, while oxidation (Met), acetylation (Protein N-term), and deamidation (NQ) were included as variable modifications. The

TMT-6 plex was used for quantitative analysis, and the data were filtered to meet the required FDR of <1%.

Molecular Dynamics Simulation: MD simulations were performed using the GROMACS 2018.4 software. Water molecules were simulated using a simple point charge model. A protein-ligand complex was contained in the center of a cub box with a side length of 12 nm, and the distance from each atom to the box wall was >1 nm. The box was randomly filled with water molecules, and counter ions were added to maintain the electrical neutrality of the system. For optimization, the simulation of energy minimization was completed using the steepest descent algorithm. In brief, only the structure and position of the water molecules were changed, and the protein structure remained unchanged. Subsequently, all the water molecules moved freely, and the system was equilibrated using a restrictive MD simulation under canonical and isothermalisobaric ensembles. Thereafter, the stability of the protein structure was examined using the classic AMBER99SB-ILDN force field, and ligands were parameterized with a generation amber force field. A Verlet shuffled frog-leaping algorithm was applied to solve Newtonian motion equations with an integral step of 2 fs. For the calculation of the van der Waals force, the Lennard-Jones function was adopted, and the non-bonded truncation distance was defined as 1.4 nm. Atomic bond lengths were restrained with the LINCS algorithm, and the long-range electrostatic interaction was calculated using the particle mesh Ewald method, with the width set at 0.16 nm. MD simulations were performed under a periodical boundary condition. First, the simulation was conducted under an isothermal-isobaric ensemble at a temperature of 310 K and a pressure of 1 atmosphere for 100 ns. The temperature and pressure were controlled with a V-rescale thermostat and Parrinello-Rahman barostat with coupling constant values of 0.1 and 2 ps, respectively. Next, the temperature was increased from 310 to 323 K, with the other parameters unchanged.

Cytotoxicity Assay: Fibroblast cells (NIH-3T3) were used to perform Thiazolyl Blue Tetrazolium Bromide (MTT) assay. Briefly, NIH-3T3 cells (200  $\mu L$ ,  $10^5$  cells  $mL^{-1}$ ) were seeded into 96-well plates. After 1 day of culture, the medium was refreshed by 200  $\mu L$  of PLGA MPs (4 mg  $mL^{-1}$  in medium) and 200  $\mu L$  of Gen-PLGA MPs (4 mg  $mL^{-1}$  in medium), respectively. Cells cultured in normal medium were set as blank control group. After culturing for 1 day, the medium was replaced by 150  $\mu L$  MTT solution (0.5 mg  $mL^{-1}$  in PBS) and the cells were further cultured for 4 h to form formazan. Afterward, the MTT solution was refreshed with 100  $\mu L$  of dimethyl sulfoxide under continuous shaking to dissolve the formazan. Finally, the absorbance at 490 nm was measured using a microplate reader (SpectraMax i3, Molecular Devices).

Hemolysis Test: The RBCs were collected from fresh blood of rat by refrigerated centrifugation at 3000 rpm for 10 min. The obtained RBCs sediment was then rinsed three times with saline and finally diluted to the concentration of 5% v/v with saline. Subsequently, 500  $\mu L$  of the diluted RBCs were incubated with 500  $\mu L$  of PLGA MPs (4 mg mL $^{-1}$  in saline) and 500  $\mu L$  of Gen-PLGA MPs (4 mg mL $^{-1}$  in saline) at 37 °C for 4 h. Thereafter, the treated RBCs mixture was centrifuged at 3000 rpm for 10 min and photographed. Last, the supernatant was collected and the absorbance at 540 nm was measured using a microplate reader (SpectraMax i3, Molecular Devices).

In Vivo UTI Model: To evaluate the in vivo efficacy of MWH, adult male Sprague-Dawley rats (n = 6 per group) were randomly divided into four groups (saline, Gen, PLGA MPs, and Gen-PLGA MPs treatment groups). On day 0, the rats were anaesthetized and inoculated with 500-µL MDR E. coli bacterial suspension at concentrations of  $1-3 \times 10^6$  CFU via the urethra into the bladder. The rats were subjected to different treatments 1 h after infection. The Gen treatment group was injected with 500  $\mu L$  of Gen solution (0.38 mg  $\mbox{mL}^{-1}$ , drug loading dose) into the bladder via the urethra. The saline, PLGA MPs, and Gen-PLGA MPs treatment groups were injected with 500  $\mu$ L of saline, 500  $\mu$ L of PLGA MPs (4 mg mL<sup>-1</sup>), and 500 μL of Gen-PLGA MPs (4 mg mL<sup>-1</sup>), respectively, via the urethra into the bladder and then irradiated with a MW physiotherapy probe (4 W, 50% duty cycle) for 10 min. A thermal image was used to record the increase in temperature during treatment. After 24 h of treatment, the clinical conditions of the rats were assessed, and the treated rats were humanely euthanized with pentobarbitone overdose. Urine, kidney, and



FUNCTIONAL

www.afm-journal.de

bladder samples were collected and quantitatively cultured onto agar for CFU counts in homogenate. Bladder samples were collected for H&E and immunofluorescence staining (TNF- $\alpha$ , IL-1 $\beta$ , and IL-6). Kidney samples were also collected for H&E and immunofluorescence staining (IL-6).

In Vivo PI Model: To further evaluate the in vivo efficacy and penetration depth of MWH, adult male Sprague-Dawley rats (n = 6 per group) were randomly divided into four groups (saline, Gen, PLGA MP, and Gen-PLGA MPs treatment groups) for the PI model. On day 0, the rats were anaesthetized and infected with intraperitoneal administration of 500- $\mu$ L MDR E. coli bacterial suspension at concentrations of 1–3  $\times$  10<sup>6</sup> CFU. The rats were subjected to different treatments 1 h after infection. The Gen treatment group was injected with 500 µL of Gen solution (0.38 mg mL<sup>-1</sup>, drug loading dose) via intraperitoneal administration. The saline, PLGA MPs, and Gen-PLGA MPs treatment groups were injected with 500  $\mu$ L of saline, 500  $\mu$ L of PLGA MPs (4 mg mL<sup>-1</sup>), and 500 μL of Gen-PLGA MPs (4 mg mL<sup>-1</sup>), respectively, via intraperitoneal administration, and then irradiated using a MW physiotherapy probe (4 W, 50% duty cycle) for 10 min. A thermal image was used to record the increase in temperature during treatment. After 24 h of treatment, the clinical conditions of the rats were assessed, and the treated rats were humanely euthanized with pentobarbitone overdose. Peritoneal fluid was collected and quantitatively cultured onto agar for CFU counts. Peritoneal tissue was collected for H&E and immunofluorescence staining (TNF- $\alpha$  and IL-1 $\beta$ ).

Statistical Analysis: All the experimental data were analyzed using mean  $\pm$  standard deviation (SD) with  $n \ge 3$ . The statistical analyses were performed using the GraphPad Prism software, with one-way analysis of variance followed by the Tukey multiple-comparisons test for multiple comparisons and a two-sample Student t-test for comparison of two groups. In addition, p values of <0.05, \*\*<0.01, \*\*\*<0.001, and \*\*\*\*\*<0.0001 were considered statistically significant.

# **Supporting Information**

Supporting Information is available from the Wiley Online Library or from the author.

#### **Acknowledgements**

This work was jointly supported by National Key R&D Program of China (2018YFA0703100), General Research Fund of Hong Kong Research Grant Council (nos. 17207719 and 17214516), Hong Kong Health and Medical Research Fund (nos.19180712, 20190422, and 21200592), Innovation and Technology Fund Partnership Research Program (PRP/030/30FX), the National Science Fund for Distinguished Youth Scholar (no. 51925104), Shenzhen Science and Technology Funding (nos. JSGG20180507183242702 and JCYJ20210324120009026), and Sanming Project of Medicine in Shenzhen "Team of Excellence in Spinal Deformities and Spinal Degeneration" (SZSM201612055). The authors thank Hubei Provincial Center for Disease Control and Prevention, Wuhan, China for approving animal experiments (Approval No. 202120168). All rats were kept and treated according to the Animal Management Rules of the Ministry of Health of the People's Republic of China and the Guidelines for the Care and Use of Laboratory Animals of China.

## **Conflict of Interest**

The authors declare no conflict of interest.

## **Data Availability Statement**

The data that support the findings of this study are available from the corresponding author upon reasonable request.

#### **Keywords**

 $\beta$ -barrel assembly machine complex, antibiotic resistance, enzymatic degradation/modification, microwave hyperthermia, multidrug-resistant *E. coli* 

Received: March 13, 2022 Revised: April 1, 2022 Published online: April 29, 2022

- [1] A. Fleming, Br. J. Exp. Pathol. 1929, 10, 226.
- [2] T. S. Crofts, A. J. Gasparrini, G. Dantas, Nat. Rev. Microbiol. 2017, 15, 422
- [3] J. O'Neill, Tackling Drug-resistant Infections Globally: Final Report and Recommendations, Wellcome Trust, London 2016.
- [4] S. M. Schrader, J. Vaubourgeix, C. Nathan, Sci. Trans. Med. 2020, 12, eaaz6992.
- [5] A. J. Lopatkin, S. C. Bening, A. L. Manson, J. M. Stokes, M. A. Kohanski, A. H. Badran, A. M. Earl, N. J. Cheney, J. H. Yang, J. J. Collins, *Science* 2021, 371, eaba0862.
- [6] E. D. Brown, G. D. Wright, Nature 2016, 529, 336.
- [7] K. Shatalin, A. Nuthanakanti, A. Kaushik, D. Shishov, A. Peselis, I. Shamovsky, B. Pani, M. Lechpammer, N. Vasilyev, E. Shatalina, D. Rebatchouk, A. Mironov, P. Fedichev, A. Serganov, E. Nudler, Science 2021, 372, 1169.
- [8] A. G. Levine, 125 Questions: Exploration and Discovery, Science/ AAAS Custom Publishing Office, Washington 2021.
- [9] E. Tacconelli, E. Carrara, A. Savoldi, S. Harbarth, M. Mendelson, D. L. Monnet, C. Pulcini, G. Kahlmeter, J. Kluytmans, Y. Carmeli, M. Ouellette, K. Outterson, J. Patel, M. Cavaleri, E. M. Cox, C. R. Houchens, M. L. Grayson, P. Hansen, N. Singh, U. Theuretzbacher, N. Magrini, WHO Pathogens Priority List Working Group, Lancet Infect. Dis. 2018, 18, 318.
- [10] K. S. Singh, R. Sharma, P. A. N. Reddy, P. Vonteddu, M. Good, A. Sundarrajan, H. Choi, K. Muthumani, A. Kossenkov, A. R. Goldman, H. Y. Tang, M. Totrov, J. Cassel, M. E. Murphy, R. Somasundaram, M. Herlyn, J. M. Salvino, F. Dotiwala, *Nature* 2021, 589, 597.
- [11] M. C. Sousa, Nature 2019, 576, 389.
- [12] R. E. W. Hancock, Trends Microbiol. 1997, 5, 37.
- [13] J. Vergalli, I. V. Bodrenko, M. Masi, L. Moynie, S. Acosta-Gutierrez, J. H. Naismith, A. Davin-Regli, M. Ceccarelli, B. van den Berg, M. Winterhalter, J. M. Pages, Nat. Rev. Microbiol. 2020, 18, 164.
- [14] N. Noinaj, A. J. Kuszak, J. C. Gumbart, P. Lukacik, H. Chang, N. C. Easley, T. Lithgow, S. K. Buchanan, *Nature* 2013, 501, 385.
- [15] D. Tomasek, S. Rawson, J. Lee, J. S. Wzorek, S. C. Harrison, Z. Li, D. Kahne, *Nature* **2020**, *583*, 473.
- [16] A. I. C. Höhr, C. Lindau, C. Wirth, J. Qiu, D. A. Stroud, S. Kutik, B. Guiard, C. Hunte, T. Becker, N. Pfanner, N. Wiedemann, *Science* 2018. 359, eaah6834.
- [17] E. M. Hart, A. M. Mitchell, A. Konovalova, M. Grabowicz, J. Sheng, X. Han, F. P. Rodriguez-Rivera, A. G. Schwaid, J. C. Malinverni, C. J. Balibar, S. Bodea, Q. Si, H. Wang, M. F. Homsher, R. E. Painter, A. K. Ogawa, H. Sutterlin, T. Roemer, T. A. Black, D. M. Rothman, S. S. Walker, T. J. Silhavy, Proc. Natl. Acad. Sci. U. S. A. 2019, 116, 21748.
- [18] A. Luther, M. Urfer, M. Zahn, M. Muller, S. Y. Wang, M. Mondal, A. Vitale, J. B. Hartmann, T. Sharpe, F. L. Monte, H. Kocherla, E. Cline, G. Pessi, P. Rath, S. M. Modaresi, P. Chiquet, S. Stiegeler, C. Verbree, T. Remus, M. Schmitt, C. Kolopp, M. A. Westwood, N. Desjonqueres, E. Brabet, S. Hell, K. LePoupon, A. Vermeulen, R. Jaisson, V. Rithie, G. Upert, et al., *Nature* 2019, 576, 452.
- [19] Y. Imai, K. J. Meyer, A. Iinishi, Q. Favre-Godal, R. Green, S. Manuse, M. Caboni, M. Mori, S. Niles, M. Ghiglieri, C. Honrao,



- X. Ma, J. J. Guo, A. Makriyannis, L. Linares-Otoya, N. Bohringer, Z. G. Wuisan, H. Kaur, R. Wu, A. Mateus, A. Typas, M. M. Savitski, J. L. Espinoza, A. O'Rourke, K. E. Nelson, S. Hiller, N. Noinaj, T. F. Schaberle, A. D'Onofrio, K. Lewis, *Nature* **2019**, *576*, 459.
- [20] K. M. Storek, M. R. Auerbach, H. Shi, N. K. Garcia, D. Sun, N. N. Nickerson, R. Vij, Z. Lin, N. Chiang, K. Schneider, A. T. Wecksler, E. Skippington, G. Nakamura, D. Seshasayee, J. T. Koerber, J. Payandeh, P. A. Smith, S. T. Rutherford, *Proc. Natl. Acad. Sci. U. S. A.* 2018, *115*, 3692.
- [21] M. Miethke, M. Pieroni, T. Weber, M. Bronstrup, P. Hammann, L. Halby, P. B. Arimondo, P. Glaser, B. Aigle, H. B. Bode, R. Moreira, Y. Li, A. Luzhetskyy, M. H. Medema, J. L. Pernodet, M. Stadler, J. R. Tormo, O. Genilloud, A. W. Truman, K. J. Weissman, E. Takano, S. Sabatini, E. Stegmann, H. Brotz-Oesterhelt, W. Wohlleben, M. Seemann, M. Empting, A. K. H. Hirsch, B. Loretz, C. M. Lehr, et al., Nat. Rev. Chem. 2021, 5, 726.
- [22] C. Årdal, M. Balasegaram, R. Laxminarayan, D. McAdams, K. Outterson, J. H. Rex, N. Sumpradit, Nat. Rev. Microbiol. 2020, 18, 267.
- [23] S. A. Yavari, S. M. Castenmiller, J. A. G. van Strijp, M. Croes, Adv. Mater. 2020, 32, 2002962.
- [24] R. Jamaledin, C. K. Y. Yiu, E. N. Zare, L. N. Niu, R. Vecchione, G. Chen, Z. Gu, F. R. Tay, P. Makvandi, Adv. Mater. 2020, 32, 2002129.
- [25] M. D. Disney, S. Magnet, J. S. Blanchard, P. H. Seeberger, Angew. Chem., Int. Ed. 2004, 43, 1591.
- [26] L. Tan, Z. Zhou, X. M. Liu, J. Li, Y. F. Zheng, Z. D. Cui, X. J. Yang, Y. Q. Liang, Z. Y. Li, X. B. Feng, S. L. Zhu, K. W. K. Yeung, C. Yang, X. B. Wang, S. L. Wu, Adv. Sci. 2020, 7, 1902070.
- [27] R. Agarwal, C. T. Johnson, B. R. Imhoff, R. M. Donlan, N. A. McCarty, A. J. Garcia, Nat. Biomed. Eng. 2018, 2, 841.
- [28] J. Li, X. Liu, L. Tan, Z. Cui, X. Yang, Y. Liang, Z. Li, S. Zhu, Y. Zheng, K. W. K. Yeung, X. Wang, S. Wu, Nat. Commun. 2019, 10, 4490.
- [29] Y. Q. Qiao, X. M. Liu, B. Li, Y. Han, Y. F. Zheng, K. W. K. Yeung, C. Y. Li, Z. D. Cui, Y. Q. Liang, Z. Y. Li, S. L. Zhu, X. B. Wang, S. L. Wu, Nat. Commun. 2020, 11, 4446.
- [30] E. Bronstein, L. Z. Tóth, L. Daróczi, D. L. Beke, R. Talmon, D. Shilo, Adv. Funct. Mater. 2021, 31, 2106573.
- [31] H. Tang, X. Xu, Y. Chen, H. Xin, T. Wan, B. Li, H. Pan, D. Li, Y. Ping, Adv. Mater. 2021, 33, 2006003.
- [32] K. Zhang, X. Meng, Y. Cao, Z. Yang, H. Dong, Y. Zhang, H. Lu, Z. Shi, X. Zhang, Adv. Funct. Mater. 2018, 28, 1804634.
- [33] Y. Gu, H. Li, H. Dong, Y. Zeng, Z. Zhang, N. G. Paterson, P. J. Stansfeld, Z. Wang, Y. Zhang, W. Wang, C. Dong, *Nature* 2016, 531, 64.
- [34] P. White, S. F. Haysom, M. G. Iadanza, A. J. Higgins, J. M. Machin, J. M. Whitehouse, J. E. Horne, B. Schiffrin, C. Carpenter-Platt, A. N. Calabrese, K. M. Storek, S. T. Rutherford, D. J. Brockwell, N. A. Ranson, S. E. Radford, *Nat. Commun.* 2021, 12, 4174.
- [35] J. Bakelar, S. K. Buchanan, N. Noinaj, Science 2016, 351, 180.
- [36] X. Yan, B. Yang, Y. Chen, Y. Song, J. Ye, Y. Pan, B. Zhou, Y. Wang, F. Mao, Y. Dong, D. Liu, J. Yu, Adv. Mater. 2021, 33, 2104758.

- [37] D. A. Stroud, C. Meisinger, N. Pfanner, N. Wiedemann, Science 2010, 328, 831.
- [38] R. Rodríguez-Alonso, J. Létoquart, V. S. Nguyen, G. Louis, A. N. Calabrese, B. I. Iorga, S. E. Radford, S.-H. Cho, H. Remaut, J.-F. Collet, Nat. Chem. Biol. 2020, 16, 1019.
- [39] R. Sikdar, J. H. Peterson, D. E. Anderson, H. D. Bernstein, *Nat. Commun.* 2017, 8, 1309.
- [40] L. Schnaider, S. Brahmachari, N. W. Schmidt, B. Mensa, S. Shaham-Niv, D. Bychenko, L. Adler-Abramovich, L. J. W. Shimon, S. Kolusheva, W. F. DeGrado, E. Gazit, *Nat. Commun.* 2017, 8, 1365.
- [41] P. J. F. Henderson, C. Maher, L. D. H. Elbourne, B. A. Eijkelkamp, I. T. Paulsen, K. A. Hassan, *Chem. Rev.* 2021, 121, 5417.
- [42] T. F. Durand-Reville, A. A. Miller, J. P. O'Donnell, X. Wu, M. A. Sylvester, S. Guler, R. Iyer, A. B. Shapiro, N. M. Carter, C. Velez-Vega, S. H. Moussa, S. M. McLeod, A. Chen, A. M. Tanudra, J. Zhang, J. Comita-Prevoir, J. A. Romero, H. Huynh, A. D. Ferguson, P. S. Horanyi, S. J. Mayclin, H. S. Heine, G. L. Drusano, J. E. Cummings, R. A. Slayden, R. A. Tommasi, *Nature* 2021, 597, 698.
- [43] P. Makvandi, C. Wang, E. N. Zare, A. Borzacchiello, L. Niu, F. R. Tay, Adv. Funct. Mater. 2020, 30, 1910021.
- [44] P. Kumar, E. H. Serpersu, M. J. Cuneo, Sci. Adv. 2018, 4, eaas8667.
- [45] M. Ye, Y. Zhao, Y. Wang, M. Zhao, N. Yodsanit, R. Xie, D. Andes, S. Gong, Adv. Mater. 2021, 33, 2006772.
- [46] K. Bush, P. A. Bradford, Nat. Rev. Microbiol. 2019, 17, 295.
- [47] M. Sjodt, K. Brock, G. Dobihal, P. D. A. Rohs, A. G. Green, T. A. Hopf, A. J. Meeske, V. Srisuknimit, D. Kahne, S. Walker, D. S. Marks, T. G. Bernhardt, D. Z. Rudner, A. C. Kruse, *Nature* 2018. 556. 118.
- [48] J. F. Fisher, S. Mobashery, Chem. Rev. 2021, 121, 3412.
- [49] X. Jia, J. Zhang, W. Sun, W. He, H. Jiang, D. Chen, A. I. Murchie, Cell 2013, 152, 68.
- [50] P. Kumar, P. K. Agarwal, M. B. Waddell, T. Mittag, E. H. Serpersu, M. J. Cuneo, *Angew. Chem., Int. Ed.* 2019, 58, 16260.
- [51] M. G. Iadanza, A. J. Higgins, B. Schiffrin, A. N. Calabrese, D. J. Brockwell, A. E. Ashcroft, S. E. Radford, N. A. Ranson, *Nat. Commun.* 2016, 7, 12865.
- [52] H. I. Zgurskaya, Chem. Rev. 2021, 121, 5095.
- [53] J. Larsen, C. L. Raisen, X. Ba, N. J. Sadgrove, G. F. Padilla-Gonzalez, M. S. J. Simmonds, I. Loncaric, H. Kerschner, P. Apfalter, R. Hartl, A. Deplano, S. Vandendriessche, B. Cerna Bolfikova, P. Hulva, M. C. Arendrup, R. K. Hare, C. Barnadas, M. Stegger, R. N. Sieber, R. L. Skov, A. Petersen, O. Angen, S. L. Rasmussen, C. Espinosa-Gongora, F. M. Aarestrup, L. J. Lindholm, S. M. Nykasenoja, F. Laurent, K. Becker, B. Walther, et al., Nature 2022, 602, 135.
- [54] M. Stracy, O. Snitser, I. Yelin, Y. Amer, M. Parizade, R. Katz, G. Rimler, T. Wolf, E. Herzel, G. Koren, J. Kuint, B. Foxman, G. Chodick, V. Shalev, R. Kishony, *Science* 2022, 375, 889.
- [55] A. G. Elliott, J. X. Huang, S. Neve, J. Zuegg, I. A. Edwards, A. K. Cain, C. J. Boinett, L. Barquist, C. V. Lundberg, J. Steen, M. S. Butler, M. Mobli, K. M. Porter, M. A. T. Blaskovich, S. Lociuro, M. Strandh, M. A. Cooper, *Nat. Commun.* 2020, 11, 3184.